SIAM J. Applied Dynamical Systems
Vol. 18, No. 4, pp. 1982–1999
© 2019 Society for Industrial and Applied Mathematics

An Optimal Framework for Nonfeedback Stability Control of Chaos*

Dan D. Wilson†

Abstract. While stabilization of chaotic dynamics through the application of periodic stimulation has been studied for many years, general conditions for the suppression of chaos using this nonfeedback approach have yet to be developed. Using a high-accuracy phase-amplitude reduction, system nonlinearities are directly exploited to derive conditions that are guaranteed to stabilize a chaotic system through the application of periodic stimulation; these conditions are then manipulated to achieve stabilization in an energy-optimal manner. The resulting control framework is highly adaptable and can be applied straightforwardly to systems with arbitrarily high dimension. Applications to the Lorenz equations and a forced double pendulum are illustrated. In numerical simulations, the nonfeedback method proposed here performs comparably to well-established closed-loop strategies when stabilization in the presence of noise is considered.

Key words. chaos, chase-amplitude reduction, isostables, isochrons, Floquet theory

AMS subject classifications. 34H05, 34E10, 39Dxx, 34H10

DOI. 10.1137/18M1229146

1. Introduction.

In a seminal work, [30] observed that chaotic dynamics could be suppressed by stabilizing an unstable periodic orbit embedded within a chaotic attractor. This fundamental observation set off an explosion of interest in the field of chaos control over the subsequent decades [32], [10], [22], [23], [33] with applications to neuroscience [38], [44], cardiology [36], [7], robotics [17], secure communications [8], [14], and desynchronization of limit cycle oscillators [31].

The examples provided above use feedback control to achieve stabilization. In principle, these feedback control strategies can be implemented using vanishingly small inputs as the dynamical system converges to the periodic orbit under the action of the control stimulus, making them an ideal solution for suppressing chaos. However, in practice, control strategies that require real-time feedback about a system's state can become infeasible when working with fast time scales, small length scales, or any system for which accurate real-time measurements are difficult to obtain. Additionally, noise, measurement error, and other sources of uncertainty can have an adverse affect on on these feedback control methods [1], [39].

By comparison, nonfeedback methods for chaos control are much less developed than their closed-loop counterparts. In general, nonfeedback control methods use periodic stimulation in order to stabilize an unstable periodic orbit [27], [2], [5], [35], [13], [6], [40]. These control strategies modify the orbit of the system itself, and the perturbations do not disappear as the state approaches the new orbit. Despite these limitations, nonfeedback control is generally much simpler to implement because it does not require real-time measurements about a sys-

*Received by the editors November 27, 2018; accepted for publication (in revised form) by D. Barkley September 12, 2019; published electronically November 7, 2019.
https://doi.org/10.1137/18M1229146
†Electrical Engineering and Computer Science, University of Tennessee, Knoxville, TN 37996 (dwilso81@utk.edu).

Copyright © by SIAM. Unauthorized reproduction of this article is prohibited.

Downloaded 11/08/19 to 160.36.59.48. Redistribution subject to SIAM license or copyright; see http://www.siam.org/journals/ojsa.php

Downloaded 11/08/19 to 160.36.59.48. Redistribution subject to SIAM license or copyright; see http://www.siam.org/journals/ojsa.php

tem's state. Unfortunately, theoretical understanding of these methods has been limited to low-dimensional systems with relatively simple dynamics; general conditions for suppression of chaos using nonfeedback control have yet to be developed.

This work will consider nonfeedback suppression of chaos in a general, nonlinear dynamical system of the form

$$\frac{dx}{dt} = F(x) + U(t), \tag{1}$$

where $x \in \mathbb{R}^N$, $F(x)$ represents the system dynamics, and $U(t) \in \mathbb{R}^N$ is a T_p-periodic perturbation where $|U(t)| = \mathcal{O}(\epsilon)$ with $0 \leq \epsilon \ll 1$. The analysis to follow builds upon the recently introduced notion of phase-amplitude reduction using isostable coordinates [46], [20], [49], [41], [45]. This isostable coordinate reduction approach incorporates dominant system nonlinearities while retaining analytical tractibility when applied to understand the dynamical behavior of a system with an unstable periodic orbit. The organization of this paper is as follows: section 2 provides a brief summary of recent results regarding phase-amplitude reduction using isostable coordinates for systems with stable periodic orbits. Section 3 subsequently extends the notion of phase and isostable coordinates for use with unstable periodic orbits. Section 4 uses this phase-amplitude coordinate system to derive general necessary conditions for stabilization of an unstable periodic orbit, applies these conditions to develop an optimal nonfeedback control strategy for suppression of chaos, and gives comparisons with other previously developed chaos control strategies. Section 5 provides concluding remarks.

2. Background on phase-amplitude reduction of stable limit cycles using isostable coordinates.

This section provides background information on the phase-amplitude reduction strategies using isostable coordinates that will be employed in the chaos control strategies to follow. A more detailed discussion of this coordinate framework is provided in [46] and [45]. For simplicity in presentation, it will be assumed that $U(t) = \begin{bmatrix} u(t) & 0 & \dots & 0 \end{bmatrix}^T$, but note that the analysis to follow can be applied straightforwardly without this restriction. To begin, suppose that (1) admits a stable T-periodic limit cycle solution $x^\gamma(t)$. Because the periodic orbit is topologically equivalent to a circle, locations on the limit cycle are often characterized by a phase of oscillation $x \mapsto \theta \in \mathbb{S}^1$ [50]. For initial conditions that are perturbed from the limit cycle the notion of isochrons [50], [18] can be used to extend the idea of phase to the basin of attraction of the limit cycle, $\mathcal{B}(\gamma)$. Intuitively, trajectories with different initial conditions lying on the same isochron converge as time approaches infinity. Stated more precisely, for any location $x^\delta \in \mathcal{B}(\gamma)$, its associated isochron can be defined as the unique value $\theta^a(x^\delta) \in [0, 2\pi)$ that solves

$$\lim_{t\to\infty} \left| \nu(t, x^\delta) - \nu\left(t + \frac{T}{2\pi}\theta^a(x^\delta), x^\gamma(0)\right)\right| = 0, \tag{2}$$

where ν represents the unperturbed flow. Here, θ^a is an asymptotic phase that is defined according to the infinite time decay of solutions to the periodic orbit. This notion of asymptotic phase can be used to yield a phase reduction [21], [50], [12] of the form

$$\dot{\theta}^a = \omega + Z(\theta^a)u(t), \tag{3}$$

where $\omega = 2\pi/T$ and $Z(\theta^a)$ is the phase response curve which captures the effect of external perturbations.

Copyright © by SIAM. Unauthorized reproduction of this article is prohibited.

Downloaded 11/08/19 to 160.36.59.48. Redistribution subject to SIAM license or copyright; see http://www.siam.org/journals/ojsa.php

Equation (2) is accurate to leading order ϵ. In many cases (including in the chaos control framework to follow) it is necessary to use a higher order accuracy version of the phase reduced equations. To do so, the behavior in directions transverse to the limit cycle of (1) must be explicitly considered. While there are various choices for coordinate systems that accomplish this goal (see also [42], [3]), an isostable coordinate framework often results in a high accuracy, analytically tractable reduced order set of equations. Toward stating the standard definition of isostable coordinates, let Γ_0^a denote the $\theta^a(x) = 0$ isochron. From the definition of isochrons (2), the return time from Γ_0^a to Γ_0^a is T so that this surface can be used to define the Poincaré map

$$\begin{aligned} P : \Gamma_0^a &\to \Gamma_0^a, \\ x &\to \nu(T, x). \end{aligned} \tag{4}$$

Linearizing about the fixed point x_0 of the Poincaré map (corresponding to the intersection of $x^\gamma(t)$ and Γ_0^a) yields

$$\nu(T, x) = x_0 + J_p(x - x_0), \tag{5}$$

where J_p is the Jacobian of $\nu(T, x)$ evaluated at x_0 (not to be confused with the Jacobian of the vector field). Let λ_k for $k = 1, \ldots, N$ be Floquet multipliers of the periodic orbit (i.e., the eigenvalues of J_p). Floquet multipliers will be ordered so that $\lambda_N = 1$. (This is the Floquet multiplier corresponding to time translation in the direction of the periodic orbit.) Additionally, $|\lambda_k| < 1$ for $k = 1, \ldots, N-1$ because the periodic orbit is stable. Provided J_p is diagonalizable, by defining right (resp., left) eigenvectors v_k (resp., w_k^T) associated with λ_k, isostable coordinates can be defined as in [46]:

$$\psi_k^a(x) = \lim_{j\to\infty} \left[w_k^T (\nu(t_\Gamma^j, x) - x_0) \exp(-\kappa_k t_\Gamma^j) \right] \quad \text{for } k = 1, \ldots, N-1, \tag{6}$$

where $\kappa_k = \ln(\lambda_k)/T < 0$ is a Floquet exponent of the limit cycle, and t_Γ^j is the jth return time to Γ_0 under the flow. Here much like the asymptotic phase, ψ_j^a is an asymptotic isostable coordinate that is defined according to the infinite time approach to the periodic orbit. Intuitively, each ψ_j^a coordinate can be thought of as a signed distance from the periodic orbit in a specific direction. A particularly useful property of these isostable coordinates is that they decay exponentially in the absence of external perturbations; starting with the definition (6) one can show $\dot{\psi}_j^a = \kappa_j \psi_j^a$ when $u(t) = 0$. This exponential decay ultimately results in a second order accurate transformation to phase-amplitude coordinates that remains analytically tractable. In [46], it was shown that isostable coordinates can be used to obtain a second order accurate phase-amplitude reduction of the form (cf., [20])

$$\begin{aligned} \dot{\theta}^a &= \omega + \left[Z(\theta^a) + \sum_{k=1}^{M} \left(\psi_k^a B^k(\theta^a) \right) \right] u(t), \\ \dot{\psi}_j^a &= \kappa_j \psi_j^a + \left[I_j(\theta^a) + \sum_{k=1}^{M} \left(\psi_k^a C_j^k(\theta^a) \right) \right] u(t), \\ & j = 1, \ldots, M. \end{aligned} \tag{7}$$

Copyright © by SIAM. Unauthorized reproduction of this article is prohibited.

Downloaded 11/08/19 to 160.36.59.48. Redistribution subject to SIAM license or copyright; see http://www.siam.org/journals/ojsa.php

Here, $Z(\theta^a)$ is the same as the phase response curve from (3) and $I_j(\theta^a)$ is the isostable response curve which characterizes the first order accurate influence of external perturbations to the isostable coordinate ψ_j^a. Additionally $B^k(\theta^a)$ and $C_j^k(\theta^a)$ provide corrections to the reduced dynamics when the state is perturbed from the periodic orbit. When Floquet exponents are negative and large in magnitude, the associated isostable coordinates are often assumed to be zero, yielding a reduction in dimensionality compared to the original equations and hence $M \leq N-1$ [49], [46], [45].

3. Phase and isostable coordinates for unstable periodic orbits. As illustrated above, previous authors have defined phase and isostable coordinates with respect to the infinite time approach of a trajectory to a limit cycle solution [46], [41]. This notion works well for stable limit cycles and can also be implemented when all nontrivial Floquet exponents are unstable by computing the convergence to the periodic orbit in reverse time. However, for periodic orbits with saddle type stability considered in the applications to follow (i.e., with some Floquet exponents having positive and some having negative real parts) most initial conditions do not converge to the periodic orbit and the definition of isostable coordinates needs to be modified. Note that the following definitions of phase and isostable coordinates are distinct from those presented in [47].

In the derivation and in the applications to follow, the notation θ and ψ_j will be used to denote phase and isostable coordinates, respectively, that are defined according to finite time behavior (as opposed to the definitions θ^a and ψ^a that are defined according to asymptotic behavior). To begin, near an unstable T-periodic orbit, the dynamics can be approximated by linearizing the differential equation (1) about the unstable orbit $x^\gamma(t)$

$$\frac{d\Delta x}{dt} = J(x^\gamma(t))\Delta x + \mathcal{O}(|\Delta x|^2), \tag{8}$$

where $\Delta x(t) = x(t) - x^\gamma(t)$ and $J(x^\gamma(t)) \in \mathbb{R}^{N\times N}$ is the Jacobian of the vector field (1) evaluated at $x^\gamma(t)$. Because (8) is T-periodic, the structure of solutions near the periodic orbit can be represented using Floquet theory [16], [24] as follows:

$$x(t) = x^\gamma(t) + \sum_{j=1}^{N-1} c_j e^{\kappa_j t} q_j(t) + \mathcal{O}(|\Delta x|^2), \tag{9}$$

where $q_j(t) \in \mathbb{R}^N$ are T-periodic, c_j are constants chosen to satisfy initial conditions, and κ_j are nonzero Floquet exponents. Note that the term $q_N(t)c_N$ corresponding to the unit Floquet multiplier of the periodic orbit (with a corresponding Floquet exponent $\kappa_N = 0$) has been absorbed into $x^\gamma(t)$ in the above equation. In contrast to the previous section, unstable periodic orbits are considered so that there is no restriction on the sign of each κ_j. Using the relationship (9), Γ_0, a $\theta = 0$ level set will be defined according to

$$\Gamma_0 = \left\{ x \in \mathbb{R}^N | x = x^\gamma(0) + \sum_{j=1}^{N-1} c_j q_j(0) \right\}. \tag{10}$$

With (10) in mind, finite time phase coordinates at any location can be defined according to

$$\theta(x) = \frac{2\pi(T - t_\Gamma)}{T}, \tag{11}$$

Copyright © by SIAM. Unauthorized reproduction of this article is prohibited.

Downloaded 11/08/19 to 160.36.59.48. Redistribution subject to SIAM license or copyright; see http://www.siam.org/journals/ojsa.php

where t_Γ is defined as the first crossing of the Γ_0 level set under the flow. Next, define the matrix $V \in \mathbb{R}^{N\times N}$ so that the jth column corresponds to $q_j(0)$. Additionally, w_j^T for $1 \le j \le N$ is taken to be the jth row of the matrix V^{-1} so that $w_j^T q_i(0) = 1$ for $i = j$ and zero otherwise. Note that the vectors w_j^T defined above are identical to the left eigenvalues of J_p from (5) when taking x_0 to be the intersection of $x^\gamma(t)$ and the Γ_0 level set. For any nonzero value of κ_j, an isostable coordinate can be defined analogously to (6)

$$\psi_j(x) = w_j^T(x_\Gamma - x_0)\exp(-\kappa_j t_\Gamma), \tag{12}$$

where x_Γ denotes the location of the first crossing of the Γ_0 level set under the flow. These coordinates are defined for all x near the periodic orbit, and not just on the Γ_0 level set. Compared with (6), the isostable coordinates here are defined with respect to a single crossing of the Γ_0 level set and not the infinite time behavior. This definition is necessary when considering periodic orbits with saddle type stability because only a small subset of initial conditions converge to the periodic orbit, making infinite time definitions unusable. As noted in both [41] and [49], as a consequence of definition (12), $\psi_i(x(t_\Gamma^+)) = \psi_i(x(t_\Gamma^-)) + \mathcal{O}(|\Delta x|^2)$, i.e., there is a small discontinuity in the ψ_j coordinate across the Γ_0 level set. At locations close enough to the periodic orbit, however, this does not preclude the use of an isostable reduced equation of a form similar to (7) as illustrated below.

When $|\Delta x| = \mathcal{O}(\epsilon)$, there are many similarities between resulting phase-amplitude reduced equations when using the finite time and asymptotic definitions of phase and isostables. By direct differentiation of (11) and (12), one can show that for any location $x \notin \Gamma_0$, in the absence of perturbation $\dot\theta = 2\pi/T = \omega$ and show that $\dot\psi_j = \kappa_j\psi_j$. Consider a second order accurate transformation of (1) to finite time phase and isostable coordinates:

$$\begin{aligned}\dot\theta &= \omega + (\nabla_{x^\gamma(\theta)}\theta + H_{\theta,x^\gamma(\theta)}\Delta x)^T U(t),\\ \dot\psi_j &= \kappa_j\psi_j + (\nabla_{x^\gamma(\theta)}\theta + H_{\psi_j,x^\gamma(\theta)}\Delta x)^T U(t).\end{aligned} \tag{13}$$

Here, $H_{\theta,x^\gamma(\theta)}$ and $H_{\psi_j,x^\gamma(\theta)}$ represent the Hessian matrices of partial derivatives of θ and ψ_j, respectively, and $\nabla_{x^\gamma(\theta)}\theta$ and $\nabla_{x^\gamma(\theta)}\psi_j$ represent the gradients of θ and ψ_j, respectively, each evaluated at $x^\gamma(\theta)$ on the periodic orbit. Equation (13) is valid for all $x \notin \Gamma_0$ where the phase and isostable coordinates are continuous. By using (9) and (12), and recalling that $w_j^T q_i = 1$ for $i = j$ and zero otherwise, one can show that to leading order $|\Delta x|^2$, c_j from (9) equals $\psi_j(x)$. With this information, (9) can be rewritten as

$$x(t) = x^\gamma(\theta(t)) + \sum_{j=1}^{n-1} q_j(\theta(t))\psi_j + \mathcal{O}(|\Delta x|^2), \tag{14}$$

or equivalently,

$$\Delta x(t) = \sum_{j=1}^{n-1} q_j(\theta(t))\psi_j + \mathcal{O}(|\Delta x|^2). \tag{15}$$

Substituting (15) into (13) yields the familiar second order accurate phase-amplitude reduced

Copyright © by SIAM. Unauthorized reproduction of this article is prohibited.

Downloaded 11/08/19 to 160.36.59.48. Redistribution subject to SIAM license or copyright; see http://www.siam.org/journals/ojsa.php

equations

$$\dot{\theta} = \omega + \left[Z(\theta) + \sum_{k=1}^{M} \left(\psi_k B^k(\theta) \right) \right] u(t),$$

$$\dot{\psi}_j = \kappa_j \psi_j + \left[I_j(\theta) + \sum_{k=1}^{M} \left(\psi_k C_j^k(\theta) \right) \right] u(t),$$

$$j = 1, \ldots, N-1 \tag{16}$$

with $Z(\theta) \equiv e_1^T \nabla_{x^\gamma(\theta)} \theta$, $I_j(\theta) \equiv e_1^T \nabla_{x^\gamma(\theta)} \psi_j$, $B^k(\theta) \equiv e_1^T H_{\theta, x^\gamma(\theta)} q_k(\theta)$, and $C_j^k(\theta) \equiv e_1^T H_{\psi_j, x^\gamma(\theta)} q_k(\theta)$, where $e_1^T = \begin{bmatrix} 1 & 0 & \ldots & 0 \end{bmatrix}$.

In order to calculate the terms of this reduction, a similar strategy as used in [46] can be employed (which itself is inspired by [4]). Consider a small magnitude perturbation Δx to a trajectory on the periodic orbit at $t = 0$. Supposing that $u = 0$ for all $t > 0$, letting Δx correspond to the difference between the perturbed trajectory and the periodic orbit, second order expansion yields

$$\frac{d\Delta x(t)}{dt} = J(x^\gamma(t))\Delta x(t) + \frac{1}{2} \begin{bmatrix} \Delta x^T(t) H_1(x^\gamma(t)) \\ \vdots \\ \Delta x^T(t) H_n(x^\gamma(t)) \end{bmatrix} \Delta x(t) + \mathcal{O}(|\Delta x|^3), \tag{17}$$

where $H_i(x)$ is the Hessian of the ith element of F. Additionally, for any $x \notin \Gamma_0$, the phase shift due to the perturbation at $t = 0$ can be written as

$$\Delta\theta = (\nabla_{x^\gamma(t)} \theta)^T \Delta x + \frac{1}{2} \Delta x^T H_{\theta, x^\gamma(t)} \Delta x + \mathcal{O}(|\Delta x|^3). \tag{18}$$

Taking the time derivative of (18) (noting that $d\Delta\theta/dt = 0$ along any trajectory short enough so that it does not intersect the Γ_0 isochron), collecting $\mathcal{O}(|\Delta x|)$ terms, and manipulating yields the familiar adjoint equation (cf., [4], [11])

$$\frac{d\nabla_{x^\gamma(t)} \theta}{dt} = -J(x^\gamma(t))^T \nabla_{x^\gamma(t)} \theta. \tag{19}$$

Collecting $\mathcal{O}(|\Delta x|^2)$ terms and manipulating yields (cf., [46])

$$\frac{dH_{\theta, x^\gamma(t)}}{dt} = -\sum_{k=1}^{N} \left[Z^k(x^\gamma(t)) H_k(x^\gamma(t)) \right] - J^T(x^\gamma(t)) H_{\theta, x^\gamma(t)} - H_{\theta, x^\gamma(t)} J(x^\gamma(t)), \tag{20}$$

where $Z^k(x^\gamma(t)) \equiv \partial\theta/\partial x_k$ evaluated on the periodic orbit. The phase response curve, $Z(\theta(t))$, can be obtained by finding the periodic solution to (19) subject to to the normalizing condition $F(x^\gamma(t))^T \nabla_{x^\gamma(t)} \theta = \omega$. The Hessian can be obtained by finding the periodic solution to (20) subject to the normalizing condition $-J(x^\gamma(t))^T \nabla_{x^\gamma(t)} \theta = H_{\theta, x^\gamma(t)} F(x^\gamma(t))$.

Using an analogous strategy detailed in [46], it can be shown that the reduced equations associated with the isostable coordinates obey

$$\frac{d\nabla_{x^\gamma(t)} \psi_j}{dt} = (\kappa_j \text{diag}(1, \ldots, 1) - J(x^\gamma(t))^T) \nabla_{x^\gamma(t)} \psi_j, \tag{21}$$

Copyright © by SIAM. Unauthorized reproduction of this article is prohibited.

and

$$\frac{dH_{\psi_j,x^\gamma(t)}}{dt} = -\sum_{k=1}^{N}\left[I_j^k(x^\gamma(t))H_k(x^\gamma(t))\right] - J^T(x^\gamma(t))H_{\psi_j,x^\gamma(t)} - H_{\psi_j,x^\gamma(t)}J(x^\gamma(t)) + \kappa_j H_{\psi_j,x^\gamma(t)}, \tag{22}$$

where $\mathrm{diag}(1,\ldots,1)$ is an appropriately sized identity matrix and $I_j^k(x^\gamma(t)) \equiv \partial\psi_j/x_k$ evaluated on the periodic orbit. The isostable response curve $I_j(\theta(t))$ can be obtained by finding the periodic solution to (21) subject to the normalizing condition $q_j(0)^T\nabla_{x^\gamma(0)}\psi_j = 1$. Likewise, $H_{\psi_j,x^\gamma(t)}$ is the periodic solution of (22) subject to the normalizing condition $\left(\kappa_j\mathrm{diag}(1,\ldots,1) - J(x^\gamma(t))^T\right)\nabla_{x^\gamma(t)}\psi_j = H_{\psi_j,x^\gamma(t)}F(x^\gamma(t))$.

Once solutions to $H_{\theta,x^\gamma(\theta)}$ and $H_{\psi_j,x^\gamma(\theta)}$ have been obtained using (20) and (22), respectively, the functions $B^k(\theta)$ and $C_j^k(\theta)$ can be determined according to the definitions given after (16). Alternatively, noting that the relationships (20) and (22) are identical to the relationships used to calculate the Hessians as part of the phase-amplitude reduction when using asymptotic phase and amplitude coordinates, [45] discusses strategies that can be used to calculated $B^k(\theta)$ and $C_j^k(\theta)$ directly. Such methods are generally easier to implement when working with high-dimensional systems.

4. Optimal stabilization of unstable periodic orbits using phase and isostable coordinate transformations. Suppose that (1) has a chaotic attractor, and embedded within this attractor is an unstable, T-periodic orbit. In order to study the dynamics in a more analytically tractable coordinate system with respect to this orbit, finite time phase and isostable coordinates (11) and (12) will be used.

Using (16) as a starting point, conditions required for $u(t)$ to stabilize the underlying periodic orbit will be derived. To begin, suppose the necessary functions in (16) have already been computed for an unstable periodic orbit of (1) using methods from section 3. Recalling that $u(t)$ is a T_p-periodic perturbation, a rotating reference frame will be used where $\phi = \theta - \omega_p t$ and $\omega_p = 2\pi/T_p$ to yield

$$\begin{aligned}\dot{\phi} &= \Delta\omega + \left[Z(\phi+\omega_p t) + \sum_{k=1}^{M}\left(\psi_k B^k(\phi+\omega_p t)\right)\right]u(t),\\ \dot{\psi}_j &= \kappa_j\psi_j + \left[I_j(\phi+\omega_p t) + \sum_{k=1}^{M}\left(\psi_k C_j^k(\phi+\omega_p t)\right)\right]u(t),\\ j &= 1,\ldots,M,\end{aligned} \tag{23}$$

where $\Delta\omega = \omega - \omega_p$. Here, $\Delta\omega$ and each ψ_j are assumed to be $\mathcal{O}(\epsilon)$ terms. Equation (23) is T_p-periodic and of the general form $\dot{v} = \epsilon Q(v,t)$ so that formal averaging techniques can be applied [37], [19] to approximate (23) as

$$\begin{aligned}\dot{\Phi} &= \Delta\omega + \sigma(\Phi) + \sum_{k=1}^{M}\left(\Psi_k\beta_k(\Phi)\right),\\ \dot{y} &= (A + E(\Phi))y + p(\Phi),\end{aligned} \tag{24}$$

Copyright © by SIAM. Unauthorized reproduction of this article is prohibited.

Downloaded 11/08/19 to 160.36.59.48. Redistribution subject to SIAM license or copyright; see http://www.siam.org/journals/ojsa.php

Downloaded 11/08/19 to 160.36.59.48. Redistribution subject to SIAM license or copyright; see http://www.siam.org/journals/ojsa.php

where

$$y = \begin{bmatrix} \Psi_1 \\ \Psi_2 \\ \vdots \\ \Psi_M \end{bmatrix}, \; A = \begin{bmatrix} \kappa_1 & & & \\ & \kappa_2 & & \\ & & \ddots & \\ & & & \kappa_M \end{bmatrix}, \; E(\Phi) = \begin{bmatrix} \alpha_{1,1}(\Phi) & \alpha_{1,2}(\Phi) & \dots & \alpha_{1,M}(\Phi) \\ \alpha_{2,1}(\Phi) & \alpha_{2,2}(\Phi) & \dots & \alpha_{2,M}(\Phi) \\ \vdots & \vdots & \ddots & \vdots \\ \alpha_{M,1}(\Phi) & \alpha_{M,1}(\Phi) & \dots & \alpha_{M,M}(\Phi) \end{bmatrix}, \; p(\Phi) = \begin{bmatrix} \mu_1(\Phi) \\ \mu_2(\Phi) \\ \vdots \\ \mu_M(\Phi) \end{bmatrix}$$

with $\sigma(\Phi) = \frac{1}{T_p}\int_0^{T_p} Z(\Phi+\omega_p t)u(t)dt$, $\beta_k(\Phi) = \frac{1}{T_p}\int_0^{T_p} B^k(\Phi+\omega_p t)u(t)dt$, $\mu_k(\Phi) = \frac{1}{T_p}\int_0^{T_p} I_k(\Phi+\omega_p t)u(t)dt$, $\alpha_{j,k}(\Phi) = \frac{1}{T_p}\int_0^{T_p} C_j^k(\Phi+\omega_p t)u(t)dt$. As explained in [37], fixed points of (24) correspond to periodic orbits of (23) with the same stability.

For the moment, assume that all κ_i are real-valued. (Complex-valued κ_i will be considered momentarily.) Toward determination of conditions that guarantee the stability of (24), and hence the stability of (23), the dynamics must remain close to the unstable periodic orbit so that the phase-amplitude reduction is valid. This can be mandated by requiring $\mu_i(\Phi_0) = 0$ for $i = 1, \dots, M$. With this requirement $\Psi_k = 0$ at any fixed point of (24). With the aforementioned constraint, stable fixed points of (24) will also require $\sigma(\Phi_0) = -\Delta\omega$ with $d\sigma/d\Phi|_{\Phi_0} < 0$. Finally, stability in (24) will require the eigenvalues of $A + E(\Phi)$ to be strictly negative. It will be assumed that κ_i are unique (i.e., simple). Recalling that the matrix $E(\Phi)$ is comprised of order ϵ terms, the eigenvalues of $A + E(\Phi)$ are [9]

$$\begin{aligned} \mathrm{eig}(A+E) &= \kappa_i + w_i^T E v_i/(w_i^T v_i) + \mathcal{O}(\epsilon^2), \\ &= \kappa_i + e_i^T E e_i + \mathcal{O}(\epsilon^2), \\ &= \kappa_i + \alpha_{i,i}(\Phi) + \mathcal{O}(\epsilon^2), \text{ for } i = 1, \dots, M, \end{aligned} \tag{25}$$

where $w_i^T = e_i^T$ and $v_i = e_i$ (elements of the standard basis) are left and right eigenvectors of A corresponding to eigenvalue κ_i. Finally, if the κ_i values are not simple, an eigenvalue expansion similar to (25) could be performed that included fractional powers of ϵ [25]; this more complicated case will not be considered here. To summarize, the conditions on the T_p-periodic, $\mathcal{O}(\epsilon)$ stimulus $u(t)$ that guarantee stabilization of the underlying periodic orbit are

$$\begin{aligned} \sigma(\Phi_0) &= -\Delta\omega, \\ d\sigma/d\Phi|_{\Phi_0} &= \rho < 0, \\ \mu_i(\Phi_0) &= 0 \text{ for } i = 1, \dots, M, \\ \kappa_i + \alpha_{i,i}(\Phi_0) &= \eta_i < 0 \;\; \text{for } i = 1, \dots, M. \end{aligned} \tag{26}$$

While (26) assumes infinitesimally small perturbations, and hence a small change in the Floquet multipliers, the examples to follow illustrate that in practice the perturbations can be quite large before the effects of neglected higher order terms begin to degrade the predictive power of these stability conditions, particularly when (26) are satisfied in an energy-optimal manner.

As a first example, consider the canonical Lorenz equations [28]:

$$\begin{aligned} \dot{X} &= \sigma_L(Y - X), \\ \dot{Y} &= X(\rho_L - W) - Y + u(t) + \eta_{\text{noise}}(t), \\ \dot{W} &= XY - \beta_L W. \end{aligned} \tag{27}$$

Copyright © by SIAM. Unauthorized reproduction of this article is prohibited.

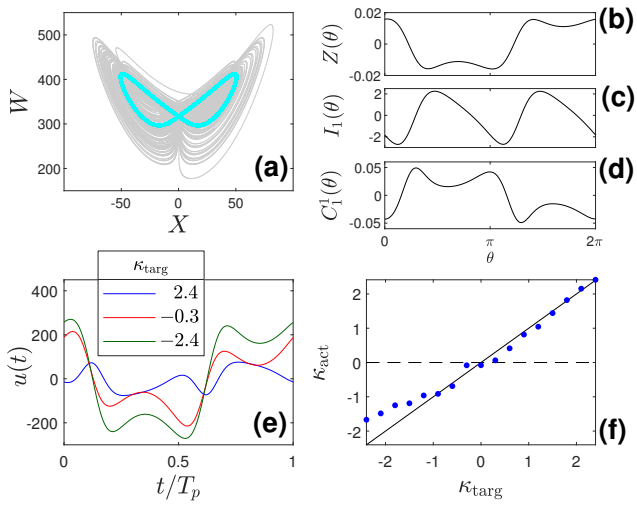

Figure 1. *Panel* (a) *shows a trajectory on the Lorenz attractor of* (27) *with an unstable periodic orbit in cyan. Panels* (b)–(d) *show functions of the reduced equations* (16) *calculated for the unstable periodic orbit. Panel* (e) *gives optimal periodic control stimuli which satisfy the conditions* (26) *where* κ_{targ} *is a target principle Floquet exponent. Panel* (f) *shows the principle Floquet exponents of the perturbed periodic orbit with periodic stimulation applied. Dots are individual datapoints and the black line, which would indicate perfect agreement, is provided for reference. The dashed horizontal line separates resulting stable and unstable orbits.*

Here X, Y, and W are nondimensional state variables, $u(t)$ is an external perturbation, and parameters $\sigma_L = 14.5$, $\rho_L = 350$, and $\beta_L = 8/3$ are chosen so that the dynamics give rise to the chaotic Lorenz attractor when $u = 0$. Independent and identically distributed noise is added in some simulations with $\eta_{\text{noise}}(t) = \sqrt{2D}\mathcal{N}(0,1)$. Panel (a) of Figure 1 shows the noiseless behavior of (27) with a trajectory on the chaotic attractor in grey and an unstable orbit with period $T = 0.3746$ shown in cyan. The nonunity Floquet multipliers for this orbit are $\lambda_1 = 2.67$ and $\lambda_2 = 4 \times 10^{-4}$. In the reduction, since one Floquet multiplier is near zero, any perturbation that influences the corresponding isostable coordinate will decay rapidly. For this reason, only one isostable coordinate will be considered with corresponding Floquet exponent $\kappa_1 = \log(\lambda_1)/T = 2.62$. Phase-amplitude reduced equations (16) are calculated for this system with curves in panels (b)–(d) corresponding to perturbations to the variable Y (e.g., $Z(\theta) = \partial\theta/\partial Y$). Using a calculus of variations approach as described in Appendix A, panel (e) shows stimuli which minimize the cost functional $\mathcal{C}[u(t)] = \int_0^T u^2(t)dt$ subject to the stabilization conditions (26) with $\eta_1 = \kappa_{\text{targ}}$ and $\rho = -0.5$. Curves in panel (e) are given with T_p chosen to yield the overall minimizer of $\mathcal{C}[u(t)]$. For optimal stimuli with a given value of κ_{targ}, panel (f) shows the principle Floquet exponent of the modified periodic orbit κ_{act} under the application of the optimal periodic stimulation. Despite $u(t)$ becoming quite large as κ_{targ} increases, the actual Floquet exponents match up well with the predicted Floquet multipliers. In the illustrations to follow the periodic stimulus that results from minimizing $\mathcal{C}[u(t)]$ subject to the stabilizing conditions (26) will be referred to as the nonfeedback stability control (NSC) strategy.

For the Lorenz equations (27), the NSC strategy with $\kappa_{\text{targ}} = -0.5$ is compared to the OGY [30] method. Briefly, the OGY method is employed by defining a Poincaré map and appropriately modifying $u(t)$ based on state feedback at each return time to the Poincaré section.

Copyright © by SIAM. Unauthorized reproduction of this article is prohibited.

Downloaded 11/08/19 to 160.36.59.48. Redistribution subject to SIAM license or copyright; see http://www.siam.org/journals/ojsa.php

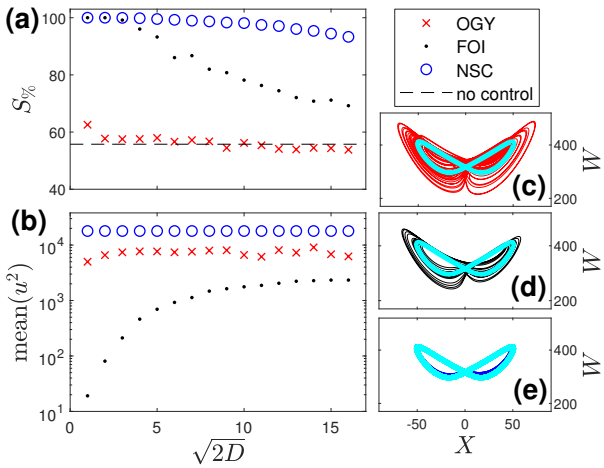

Figure 2. *Panel* (a) *shows the effectiveness of each control strategy with varying levels of noise intensity. The value $S_{\%}$ takes larger values when the trajectory stays closer to the unstable orbit over the course of a simulation, indicating more effective control. Panel* (b) *shows the average value of u^2 over each simulation. Panels* (c), (d), *and* (e) *show representative trajectories using the OGY, FOI, and NSC method, respectively, with noise intensity $\sqrt{2D} = 5$. The unstable periodic orbit is shown for reference in cyan. In panel* (e), *the trajectory and the periodic orbit are nearly indistinguishable.*

Comparisons are also given to a first order isostable (FOI) method suggested by [49], which is similar to the OGY method but uses state feedback to determine an optimal $u(t)$ to drive ψ_1 to zero over one period of oscillation. Figure 2 shows results for various noise intensities. Under the application of each control strategy, $S_{\%}$ in panel (a) represents the percentage of time over the course of 900 time units (approximately 2400 cycles) that $\min_\theta ||x(t) - x^\gamma(\theta)||_2 < 20$, where $x(t)$ is the system state and $x^\gamma(\theta)$ is the unperturbed, unstable periodic orbit. Higher values of $S_{\%}$ indicate a more effective control with fewer excursions from the unstable orbit. Panel (b) shows the mean power used during simulations and panels (c)–(e) show representative behavior in a two-dimensional cross section in simulations with $\sqrt{2D} = 5$. For this example, the OGY method does not work when noise is added, providing a negligible benefit when compared to giving no control. Additionally, the NSC outperforms the FOI method on the basis of the $S_{\%}$ metric, particularly at high noise intensities despite not requiring any state feedback. As a final note, a delayed feedback control method using an unstable controller [34] also does not work well for this control application when noise is added; results are not shown here.

As a second example, the NSC control strategy is applied to a damped, driven, double pendulum as in panel (a) of Figure 3. The dynamical equations are most easily derived using Lagrange's equations of motion [43] as illustrated in Appendix C. These equations are

$$\ddot{\upsilon}_1 = \frac{\zeta_4\zeta_5 - \zeta_2\zeta_6}{\zeta_1\zeta_4 - \zeta_2\zeta_3} + u(t),$$
$$\ddot{\upsilon}_2 = \frac{-\zeta_5\zeta_3 + \zeta_1\zeta_6}{\zeta_1\zeta_4 - \zeta_2\zeta_3}, \tag{28}$$

where $\zeta_1 = (m_1 + m_2)l_1$, $\zeta_2 = m_2 l_2 \cos(\upsilon_1 - \upsilon_2)$, $\zeta_3 = m_2 l_1 \cos(\upsilon_1 - \upsilon_2)$, $\zeta_4 = m_2 l_2$, $\zeta_5 = -m_2 l_2 \dot{\upsilon}_2^2 \sin(\upsilon_1 - \upsilon_2) - g(m_1 + m_2)\sin(\upsilon_1) - d_1\dot{\upsilon}_1/l_1 + d_2(\dot{\upsilon}_2 - \dot{\upsilon}_1)/l_1 + f_x \cos(\upsilon_1)$, $\zeta_6 =$

Copyright © by SIAM. Unauthorized reproduction of this article is prohibited.

Downloaded 11/08/19 to 160.36.59.48. Redistribution subject to SIAM license or copyright; see http://www.siam.org/journals/ojsa.php

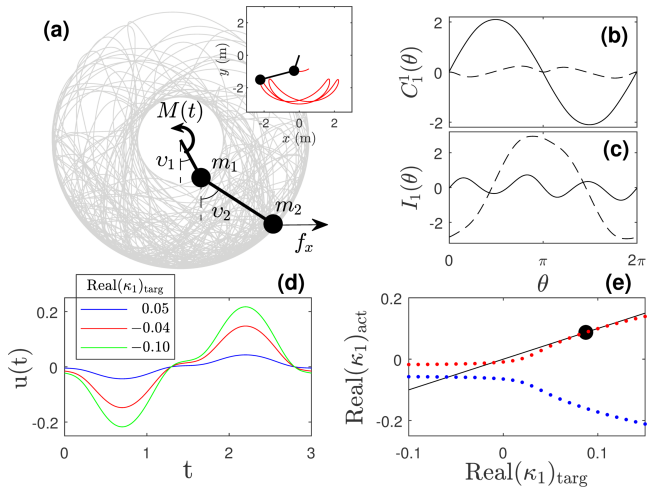

Figure 3. *Panel* (a) *shows a schematic of the forced double pendulum. A chaotic example trajectory (with* $M(t) = 0$*) of the outer point mass is shown in gray. The red curve in the upper right panel shows the unstable periodic orbit to be stabilized. Panels* (b) *and* (c) *show real (black lines) and imaginary (dashed lines) components of* $C_1^1(\theta)$ *and* $I_1(\theta)$ *corresponding to direct perturbations to* x_2*. In panel* (d)*, this information is used to calculate an energy optimal control stimulus to yield a prespecified real component of the principle Floquet multiplier. Panel* (e) *shows how the Floquet multipliers evolve under the application of the periodic optimal stimuli.* $\text{Real}(\kappa_1)_{\text{targ}}$ *denotes the prespecified value and* $\text{Real}(\kappa_1)_{\text{act}}$ *are the actual values determined by numerical simulation. Red and blue dots denote the Floquet multipliers with largest and smallest real component, respectively. The black line would indicate perfect agreement, and the black dot corresponds to the results with* $M(t) = 0$*.*

$m_2 l_1 \dot{\upsilon}_1^2 \sin(\upsilon_1 - \upsilon_2) - m_2 g \sin(\upsilon_2) - d_2(\dot{\upsilon}_2 - \dot{\upsilon}_1)/l_2 + f_x \cos(\upsilon_2)$, and $u(t) = \frac{M(t)}{l_1^2(m_1 + m_2(1-\cos^2(\upsilon_1-\upsilon_2)))}$. Here, d_1 and d_2 are damping coefficients on each pivot point, m_1 and m_2 are point masses, l_1 and l_2 are the lengths of each connection, g is the downward gravitational acceleration, $f_x = 6.56\sin(2\pi t/3)$ is a periodic horizontal force, and $M(t)$ is a moment applied directly to the first linkage. For simplicity of the control problem, the cost functional $\mathcal{C}[u(t)] = \int_0^T u^2(t)dt$ will be used to optimize the stabilizing control. Note that an alternative cost functional $\mathcal{C}_M[M(t)] = \int_0^T M^2(t)dt$ could be used instead, but would result in a more complicated optimal control problem. For the purposes of simulation and analysis, (28) is transformed to a system of 5 first order differential equations using standard techniques with $X = \begin{bmatrix} x_1 & x_2 & x_3 & x_4 & x_5 \end{bmatrix} = \begin{bmatrix} \upsilon_1 & \dot{\upsilon}_1 & \upsilon_2 & \dot{\upsilon}_2 & t \end{bmatrix}$ with time given in seconds.

With the chosen parameter set, the dynamics are chaotic with an example trajectory of the outer point mass shown in gray in panel (a) of Figure 3. An unstable periodic orbit $X^\gamma(t)$ with $T = 3$ is shown in the upper-right portion of (a) in red. The unstable Floquet multipliers are $\lambda_1, \lambda_2 = -1.19 \pm 0.53i$, with corresponding Floquet exponents $\kappa_1, \kappa_2 = 0.087 \pm 0.908i$. Given that $u(t)$ is constrained to be real, modifications to the stability conditions (26) are required. Specifically, it is required that

$$\begin{aligned} \text{Real}(\mu_1(\Phi_0)) = \text{Imag}(\mu_1(\Phi_0)) &= 0, \\ \text{Real}(\kappa_1) + \text{Real}(\alpha_{1,1}(\Phi_0)) &= \eta_1 < 0 \end{aligned} \tag{29}$$

Copyright © by SIAM. Unauthorized reproduction of this article is prohibited.

Downloaded 11/08/19 to 160.36.59.48. Redistribution subject to SIAM license or copyright; see http://www.siam.org/journals/ojsa.php

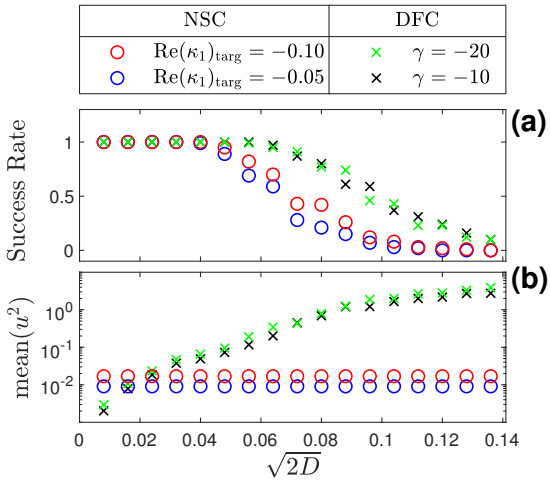

Figure 4. *Comparison of the NSC and DFC feedback strategies for the double pendulum. Panel* (a)*: The DFC method is slightly more successful than the NSC method. Panel* (b)*: At low noise intensities power consumption is similar between the two strategies. As D grows, so too does the power consumption by the DFC method.*

to ensure stability of the averaged system (24). Generally, the requirements on σ from (26) are also required, but in this example, (3) is subject to time-dependent forcing $d\theta/dx_2 = 0$, obviating this need. The reduced equations (16) are shown in panels (b) and (c) and calculated using methods described in section 3. These functions correspond to direct perturbations to the x_2 variable (e.g., $I_1 = d\psi_1/dx_2$). Due to the complex Floquet multipliers, $I_1(\theta) = \bar{I}_2(\theta)$ and $C_2^2(\theta) = \bar{C}_1^1(\theta)$, where the overbar denotes the complex conjugate. Using a calculus of variations approach as described in Appendix B, panel (d) shows stimuli which minimize the cost functional $C[u(t)]$ subject to the stability conditions (29) with $\eta_1 = \mathrm{Real}(\kappa_1)_{\mathrm{targ}}$. Upon the application of these periodic stimuli (with $T_p = 3$ seconds), panel (e) shows the real component of the resulting numerically determined Floquet exponents. The largest value of $\mathrm{Real}(\kappa_1)$ (red dots) drops at a relatively constant rate predicted by $\mathrm{Real}(\kappa_1)_{\mathrm{targ}}$ until leveling out at approximately $\mathrm{Real}(\kappa_1) = -0.018$, corresponding to a stable periodic orbit.

Finally, the NSC method is compared to the delayed feedback control (DFC) strategy [32]. Here noise is incorporated into the horizontal forcing as $f_x = 6.56\sin(2\pi t/3) + \eta_{\mathrm{noise}}(t)$ with $\eta_{\mathrm{noise}}(t)$ defined earlier. The DFC is taken to be

$$u(t) = \gamma\left[x_2(t) - x_2(t-T)\right], \tag{30}$$

where γ is a constant. This general DFC strategy has been widely studied in recent decades [39], [15]. Panel (a) of Figure 4 shows simulation results of using both the NSC and DFC strategy to stabilize the pendulum's unstable periodic orbit. To obtain the results in panel A, an initial condition starting on the periodic orbit is simulated for $T = 300$s (100 cycles). The trial is deemed successful if $\min ||X(t) - X^{\gamma}(t)||_2 < 5$ for all t and unsuccessful otherwise. Results do not differ qualitatively if a different threshold is chosen. Each datapoint represents the success rate over 100 separate trials for a given noise intensity. Panel (b) shows the mean power usage by each control strategy over each set of simulations. All times for which

Copyright © by SIAM. Unauthorized reproduction of this article is prohibited.

Downloaded 11/08/19 to 160.36.59.48. Redistribution subject to SIAM license or copyright; see http://www.siam.org/journals/ojsa.php

$||X(t) - X^{\gamma}(t)||_2 > 5$ are excluded from this calculation. At high noise intensities, the DFC strategy is slightly more successful but uses one to two orders of magnitude more energy. At low noise intensities, the performance of each controller is comparable. This level of performance is achieved by the NSC strategy despite the fact that it requires no feedback. As a final note, the OGY method is not effective at stabilizing this system even in the absence of noise.

5. Conclusions. In this work, a nonfeedback control strategy is developed for stabilizing chaotic dynamical behavior. Remarkably, in the examples provided here, this strategy performs comparably well (and sometimes better) at stabilizing the chaotic motion when tested against well-established control strategies that require real-time state feedback. In order to derive the necessary conditions (26) for stabilizing an unstable periodic orbit using periodic stimulation, the notion of phase and isostable coordinates was extended for use in unstable limit cycle oscillators with saddle type stability. Despite differences between the finite time and asymptotic definitions (for use in unstable and stable periodic orbits, respectively) both of these coordinate frameworks yield similar second order accurate phase-amplitude reduced equations that are valid close to the periodic orbit.

While many nonfeedback stabilization strategies using periodic actuation have been studied over the years, [5], [35], [13], [6], [40], the control strategy here actively exploits nonlinearities specific to a given system to achieve the control objective and can be applied in dynamical systems with arbitrarily large dimension. Ultimately, this goal is accomplished by working in an isostable coordinate system to design a periodic stimulus to stabilize the unstable Floquet multipliers in a targeted manner. While this strategy is only shown for ordinary differential equation models, it is expected that these results could extend to partial differential equations models for the control of spatiotemporal chaos.

While preliminary results are promising, significant drawbacks to the proposed DFC method still exist. Perhaps most importantly is that in order to achieve stabilization, the periodic orbit will necessarily be shifted under the application of the periodic control. This limitation could be partially mitigated by incorporating a penalty against transiently large isostable values in the cost functional that determines the optimal control stimulus, thereby limiting the deviation from the periodic orbit. Unlike with feedback methods, however, the shift in the orbit cannot be fully eliminated with the nonfeedback control strategy proposed here.

To conclude, this control strategy represents a promising new methodology for nonfeedback stabilization of chaotic behavior. It is envisioned that this strategy could be particularly useful in applications where feedback control strategies are either impractical or inadequate.[1]

Appendix A. Optimally stabilizing an unstable periodic orbit with real-valued isostable coordinates. The relations (26) provide a set of conditions that must be satisfied in order to stabilize an unstable periodic orbit using open-loop, periodic stimulation. Using calculus of variations [26], these conditions can be satisfied optimally with minimal computational effort. To illustrate this methodology, for the moment assume that all Floquet multipliers used to define the isostable coordinates are real-valued. First note that conditions (26) can

[1]This material is based upon work supported by the National Science Foundation grant CMMI-1933583.

Copyright © by SIAM. Unauthorized reproduction of this article is prohibited.

Downloaded 11/08/19 to 160.36.59.48. Redistribution subject to SIAM license or copyright; see http://www.siam.org/journals/ojsa.php

Downloaded 11/08/19 to 160.36.59.48. Redistribution subject to SIAM license or copyright; see http://www.siam.org/journals/ojsa.php

be equivalently rewritten as a set of differential equations

$$\begin{aligned}
\dot{P}_1 &= Z(\Phi_0 + \omega_p t)u(t) + \Delta\omega, \\
\dot{P}_2 &= Z'(\Phi_0 + \omega_p t)u(t), \\
\dot{Q}_i &= I_i(\Phi_0 + \omega_p t)u(t) \quad \text{for } i = 1, \ldots, M, \\
\dot{R}_i &= C_i^i(\Phi_0 + \omega_p t)u(t) + \kappa_i \quad \text{for } i = 1, \ldots, M,
\end{aligned} \tag{31}$$

where $' \equiv d/d\Phi$ subject to boundary conditions $P_1(0) = 0$, $P_1(T_p) = 0$, $P_2(0) = 0$, $P_2(T_p) = \rho T_p$, $Q_i(0) = 0$, $Q_i(T_p) = 0$, $R_i(0) = 0$, and $R_i(T_p) = \eta_i T_p$. With this transformation, the problem of finding an energy-optimal stimulus which satisfies (31) can be posed as a calculus of variations problem, i.e., finding the stimulus $u(t)$ which minimizes the cost functional

$$\begin{aligned}
\mathcal{M}[\dot{\Upsilon}, \Upsilon, u(t)] = \int_0^{T_p} \Big[& u^2(t) + \xi_{P1}\{\dot{P}_1 - Z(\Phi_0 + \omega_p t)u(t) - \Delta\omega\} + \xi_{P2}\{\dot{P}_2 - Z'(\Phi_0 + \omega_p t)u(t)\} \\
& + \sum_{i=1}^{M} \xi_{Q_i}\{\dot{Q}_i - I(\Phi_0 + \omega_p t)u(t)\} + \sum_{i=1}^{M} \xi_{R_i}\{\dot{R}_i - C_i^i(\Phi_0 + \omega_p t)u(t) - \kappa_i\} \Big] dt
\end{aligned} \tag{32}$$

with $\Upsilon = [P_1, P_2, Q_1, \ldots, Q_M, R_1, \ldots, R_M]$. Here Lagrange multipliers $\xi_{P_1}, \xi_{P_2}, \xi_{Q_i}$, and ξ_{R_i} force the dynamics to satisfy (31). Letting $\mathcal{C}$ denote the integrand of (32), the associated Euler–Lagrange equations are [26]

$$\frac{\partial \mathcal{C}}{\partial u} = \frac{d}{dt}\left(\frac{\partial \mathcal{C}}{\partial \dot{u}}\right), \tag{33}$$

$$\frac{\partial \mathcal{C}}{\partial \Upsilon} = \frac{d}{dt}\left(\frac{\partial \mathcal{C}}{\partial \dot{\Upsilon}}\right). \tag{34}$$

As detailed in [26], an optimal solution of the functional (32) will satisfy (33) and (34) with boundary conditions given as part of (31). For a general calculus of variations problem with many Lagrange multipliers, finding optimal solutions of (32) is difficult and requires the use of iterative numerical methods [48], [29]. However, for this particular problem, the evaluation of (34) reveals that the time derivative of all Lagrange multipliers equals zero. Combined with the evaluation of (33), the optimal stimulus is given by

$$u(t) = \frac{\xi_{P_1}(0)Z(\Phi_0 + \omega_p t) + \xi_{P_2}(0)Z'(\Phi_0 + \omega_p t) + \sum_{i=1}^{M}\left[\xi_{Q_i}(0)I_i(\Phi_0 + \omega_p t) + \xi_{R_i}(0)C_i^i(\Phi_0 + \omega_p t)\right]}{2}. \tag{35}$$

In addition to the dynamics of the Lagrange multipliers, evaluation of (34) returns (31). Substituting (35) into (31) yields, after some simplification, a system of $2M+2$ linear equations that can be solved for the initial values of the Lagrange multipliers that satisfy the boundary conditions. For instance, the Lagrange multipliers when considering a problem with only a single Floquet multiplier can be found as the solution to

$$\begin{bmatrix} -\Delta\omega T_p \\ \rho T_p \\ 0 \\ \eta_1 T_p - \kappa_1 T_p \end{bmatrix} = \frac{1}{2}\begin{bmatrix} \langle Z, Z\rangle & \langle Z, Z'\rangle & \langle Z, I_1\rangle & \langle Z, C_1^1\rangle \\ \langle Z', Z\rangle & \langle Z', Z'\rangle & \langle Z', I_1\rangle & \langle Z', C_1^1\rangle \\ \langle I_1, Z\rangle & \langle I_1, Z'\rangle & \langle I_1, I_1\rangle & \langle I_1, C_1^1\rangle \\ \langle C_1^1, Z\rangle & \langle C_1^1, Z'\rangle & \langle C_1^1, I_1\rangle & \langle C_1^1, C_1^1\rangle \end{bmatrix} \begin{bmatrix} \xi_{P_1}(0) \\ \xi_{P_2}(0) \\ \xi_{Q_1}(0) \\ \xi_{R_1}(0) \end{bmatrix}, \tag{36}$$

Copyright © by SIAM. Unauthorized reproduction of this article is prohibited.

where $\langle P, Q\rangle \equiv \int_0^{T_p} [P(\omega_p t)Q(\omega_p t)]\, dt$. When more Floquet multipliers are considered (36) extends naturally.

Practically in the optimization methodology presented above, as ρ and η_i are chosen to be more negative, the resulting Floquet multipliers of the perturbed solution will be more negative, resulting in dynamics that collapse more rapidly to the resulting orbit. These values can be chosen as desired. Additionally, the chosen value of Φ_0 has no bearing on the results (different values will simply shift the timing of the applied periodic stimulus but not the entrained solution itself) and for simplicity can be taken to be zero.

Appendix B. Optimal stabilization conditions with complex-valued isostable coordinates. In the case where isostable coordinates take complex values, the conditions to guarantee stabilization are slightly different, but computing optimal stimuli is still quite efficient. Consider for the moment a three-dimensional model (1) which admits a periodic orbit with two complex conjugate Floquet exponents κ_1 and $\bar{\kappa}_1$. The resulting time averaged phase-amplitude reduced equation when T_p-periodic stimulation is applied (24) is

$$\begin{aligned} \dot{\Phi} &= \Delta\omega + \sigma(\Phi) + \Psi_1\beta_1(\Phi) + \Psi_2\beta_2(\Psi), \\ \begin{bmatrix} \dot{\Psi}_1 \\ \dot{\Psi}_2 \end{bmatrix} &= \left(\begin{bmatrix} \kappa_1 & 0 \\ 0 & \overline{\kappa}_1 \end{bmatrix} + \begin{bmatrix} \alpha_{1,1}(\Phi) & \alpha_{1,2}(\Phi) \\ \alpha_{2,1}(\Phi) & \overline{\alpha}_{1,1}(\Phi) \end{bmatrix} \right) \begin{bmatrix} \Psi_1 \\ \Psi_2 \end{bmatrix} + \begin{bmatrix} \mu_1(\Phi) \\ \overline{\mu}_1(\Phi) \end{bmatrix}. \end{aligned} \tag{37}$$

The complex conjugate relationships in (37) are a direct consequence of the fact that the Floquet exponents are complex conjugate. Keeping in mind the relationship derived in (25), for (37) to have a stable fixed point corresponding to a stable periodic orbit of the unreduced system, it is required that

$$\begin{aligned} \mathrm{Real}(\kappa_1 + \alpha_{1,1}(\Phi_0)) &< 0, \\ \mathrm{Real}(\bar{\kappa}_1 + \bar{\alpha}_{1,1}(\Phi_0)) &< 0. \end{aligned} \tag{38}$$

Additionally, much like in the case with real-valued isostable coordinates, it will be required that

$$\begin{aligned} \mu_1(\Phi_0) &= 0, \\ \bar{\mu}_1(\Phi_0) &= 0. \end{aligned} \tag{39}$$

Noting that the T_p-periodic stimulus $u(t) \in \mathbb{R}$, conditions (38) and (39) will be satisfied provided

$$\begin{aligned} \mathrm{Real}(\kappa_1) + \mathrm{Real}(\alpha_{1,1}(\Phi_0)) &= \eta < 0, \\ \mathrm{Real}(\mu_1(\Phi_0)) &= 0, \\ \mathrm{Imag}(\mu_1(\Phi_0)) &= 0. \end{aligned} \tag{40}$$

The periodic orbit will then be stabilized provided the first two constraints from (26) and (40) are satisfied. Using calculus of variations and the same steps used to derive the optimal control stimulus (35) one can show that the optimal stimulus for satisfying these stability

Copyright © by SIAM. Unauthorized reproduction of this article is prohibited.

Downloaded 11/08/19 to 160.36.59.48. Redistribution subject to SIAM license or copyright; see http://www.siam.org/journals/ojsa.php

Downloaded 11/08/19 to 160.36.59.48. Redistribution subject to SIAM license or copyright; see http://www.siam.org/journals/ojsa.php

conditions is

$$u(t) = \frac{1}{2}\begin{bmatrix}\xi_1 & \xi_2 & \xi_3 & \xi_4 & \xi_5\end{bmatrix}\begin{bmatrix} Z(\Phi_0+\omega_p t) \\ Z'(\Phi_0+\omega_p t) \\ \mathrm{Real}(I_1(\Phi_0+\omega_p t)) \\ \mathrm{Imag}(I_1(\Phi_0+\omega_p t)) \\ \mathrm{Real}(C_1^1(\Phi_0+\omega_p t)) \end{bmatrix}, \tag{41}$$

where the constants ξ_i can be found as the solution to the linear equation

$$\begin{bmatrix} -\Delta\omega T_p \\ \rho T_p \\ 0 \\ 0 \\ \eta T_p - \mathrm{Real}(\kappa_1)T_p \end{bmatrix} = \frac{1}{2}A\begin{bmatrix}\xi_1\\ \xi_2\\ \xi_3\\ \xi_4\\ \xi_5\end{bmatrix}, \tag{42}$$

where $A \in \mathbb{R}^{5\times 5}$ with $A_{i,j} = \langle f_i, f_j\rangle$, $f_1 = Z$, $f_2 = Z'$, $f_3 = \mathrm{Real}(I_1)$, $f_4 = \mathrm{Imag}(I_1)$, and $f_5 = \mathrm{Real}(C_1^1)$ with $\langle\cdot,\cdot\rangle$ defined earlier.

Finally, calculation of stabilizing stimuli when the periodic orbit has multiple complex conjugate Floquet exponents or a mix of real and complex Floquet exponents extends naturally using this framework.

Appendix C. Derivation of double pendulum equations. Consider the double pendulum (28). For this system, Lagrange's equations [43] state that

$$\frac{d}{dt}\left(\frac{\partial L}{\partial \dot{q}_i}\right) - \frac{\partial L}{\partial q_i} = Q_i. \tag{43}$$

Here, $L = T - V$, where T is the kinetic energy and V is the potential energy, and Q_i are referred to as generalized forces. For the double pendulum system, let r_1 and r_2 correspond to the location of m_1 and m_2, respectively, in a Cartesian coordinate system. Noting that $r_1 = l_1\sin(\upsilon_1)\hat{\imath} - l_1\cos(\upsilon_1)\hat{\jmath}$ and $r_2 = [l_1\sin(\upsilon_1) + l_2\sin(\upsilon_2)]\hat{\imath} - [l_1\cos(\upsilon_1) + l_2\cos(\upsilon_2)]\hat{\jmath}$, one can show that

$$T = \frac{1}{2}m_1 l_1^2\dot{\upsilon}_1^2 + \frac{1}{2}m_2\left[l_1^2\dot{\upsilon}_1^2 + l_2^2\dot{\upsilon}_2^2 + 2l_1l_2\dot{\upsilon}_1\dot{\upsilon}_2\cos(\upsilon_1-\upsilon_2)\right], \tag{44}$$

$$V = -(m_1+m_2)gl_1\cos(\upsilon_1) - m_2 g l_2\cos\upsilon_2. \tag{45}$$

Additionally, generalized forces associated with the virtual work performed by the applied forces with respect to coordinates υ_1 and υ_2 are

$$\begin{aligned} Q_1 &= -d_1\dot{\upsilon}_1 + d_2(\dot{\upsilon}_2 - \dot{\upsilon}_1) + M(t) + f_x l_1\cos(\upsilon_1), \\ Q_2 &= -d_2(\dot{\upsilon}_2 - \dot{\upsilon}_1) + f_x l_2\cos(\upsilon_2). \end{aligned} \tag{46}$$

By substituting (44), (45), and (46) into (43), the equations of motion are

$$\begin{aligned} (m_1+m_2)l_1\ddot{\upsilon}_1 + m_2 l_2\ddot{\upsilon}_2\cos(\upsilon_1-\upsilon_2) + m_2 l_2\dot{\upsilon}_2^2\sin(\upsilon_1-\upsilon_2) + g(m_1+m_2)\sin(\upsilon_1) \\ = -d_1\dot{\upsilon}_1/l_1 + d_2(\dot{\upsilon}_2-\dot{\upsilon}_1)/l_1 + M(t)/l_1 + f_x\cos(\upsilon_1), \\ m_2 l_2\ddot{\upsilon}_2 + m_2 l_1\ddot{\upsilon}_1\cos(\upsilon_1-\upsilon_2) - m_2 l_1 {\dot{\upsilon}_1}^2\sin(\upsilon_1-\upsilon_2) + m_2 g\sin(\upsilon_2) \\ = -d_2(\dot{\upsilon}_2-\dot{\upsilon}_1)/l_2 + f_x\cos(\upsilon_2). \end{aligned} \tag{47}$$

Copyright © by SIAM. Unauthorized reproduction of this article is prohibited.

By defining the constants $\zeta_1 = (m_1 + m_2)l_1$, $\zeta_2 = m_2 l_2 \cos(\upsilon_1 - \upsilon_2)$, $\zeta_3 = m_2 l_1 \cos(\upsilon_1 - \upsilon_2)$, $\zeta_4 = m_2 l_2$, $\zeta_5 = -m_2 l_2 \dot{\upsilon}_2^2 \sin(\upsilon_1 - \upsilon_2) - g(m_1 + m_2)\sin(\upsilon_1) - d_1 \dot{\upsilon}_1 / l_1 + d_2(\dot{\upsilon}_2 - \dot{\upsilon}_1)/l_1 + M(t)/l_1 + f_x \cos(\upsilon_1)$, and $\zeta_6 = m_2 l_1 \dot{\upsilon}_1^2 \sin(\upsilon_1 - \upsilon_2) - m_2 g \sin(\upsilon_2) - d_2(\dot{\upsilon}_2 - \dot{\upsilon}_1)/l_2 + f_x \cos(\upsilon_2)$, (47) can be written as

$$\begin{bmatrix} \zeta_1 & \zeta_2 \\ \zeta_3 & \zeta_4 \end{bmatrix} \begin{bmatrix} \ddot{\upsilon}_1 \\ \ddot{\upsilon}_2 \end{bmatrix} = \begin{bmatrix} \zeta_5 \\ \zeta_6 \end{bmatrix}. \tag{48}$$

Equation (48) can be rewritten in the same form as (28) by multiplying both sides by the inverse of the 2-by-2 matrix.

REFERENCES

[1] S. Boccaletti, C. Grebogi, Y. C. Lai, H. Mancini, and D. Maza, *The control of chaos: Theory and applications*, Phys. Rep., 329 (2000), pp. 103–197.

[2] Y. Braiman and I. Goldhirsch, *Taming chaotic dynamics with weak periodic perturbations*, Phys. Rev. Lett., 66 (1991), 2545.

[3] P. C. Bressloff and J. N. MacLaurin, *A variational method for analyzing stochastic limit cycle oscillators*, SIAM J. Appl. Dyn. Syst., 17 (2018), pp. 2205–2233.

[4] E. Brown, J. Moehlis, and P. Holmes, *On the phase reduction and response dynamics of neural oscillator populations*, Neural Comput., 16 (2004), pp. 673–715.

[5] R. Chacon and J. D. Bejarano, *Routes to suppressing chaos by weak periodic perturbations*, Phys. Rev. Lett., 71 (1993), 3103.

[6] R. Chacon and A. M. Lacasta, *Controlling chaotic transport in two-dimensional periodic potentials*, Phys. Rev. E, 82 (2010), 046207.

[7] D. J. Christini, M. L. Riccio, C. A. Culianu, J. J. Fox, A. Karma, and R. F. Gilmour, Jr., *Control of electrical alternans in canine cardiac Purkinje fibers*, Phys. Rev. Lett., 96 (2006), 104101.

[8] K. M. Cuomo and A. V. Oppenheim, *Circuit implementation of synchronized chaos with applications to communications*, Phys. Rev. Lett., 71 (1993), pp. 65–68.

[9] J. W. Demmel, *Applied Numerical Linear Algebra*, SIAM, Philadelphia, 1997.

[10] W. L. Ditto, S. N. Rauseo, and M. L. Spano, *Experimental control of chaos*, Phys. Rev. Lett., 65 (1990), 3211.

[11] G. B. Ermentrout and N. Kopell, *Multiple pulse interactions and averaging in systems of coupled neural oscillators*, J. Math. Biol., 29 (1991), pp. 195–217.

[12] G. B. Ermentrout and D. H. Terman, *Mathematical Foundations of Neuroscience*, Interdiscip. Appl. Math. 35, Springer, New York, 2010.

[13] A. Farshidianfar and A. Saghafi, *Identification and control of chaos in nonlinear gear dynamic systems using Melnikov analysis*, Phys. Lett. A, 378 (2014), pp. 3457–3463.

[14] M. Feki, *An adaptive chaos synchronization scheme applied to secure communication*, Chaos Solitons Fractals, 18 (2003), pp. 141–148.

[15] A. L. Fradkov and R. J. Evans, *Control of chaos: Methods and applications in engineering*, Annu. Rev. Control, 29 (2005), pp. 33–56.

[16] R. Grimshaw, *Nonlinear Ordinary Differential Equations*, Vol. 2, CRC Press, Baca Raton, FL, 1993.

[17] H. Gritli, S. Belghith, and N. Khraief, *Ogy-based control of chaos in semi-passive dynamic walking of a torso-driven biped robot*, Nonlinear Dynam., 79 (2015), pp. 1363–1384.

[18] J. Guckenheimer, *Isochrons and phaseless sets*, J. Math. Biol., 1 (1975), pp. 259–273.

[19] J. Guckenheimer and P. Holmes, *Nonlinear Oscillations, Dynamical Systems, and Bifurcations of Vector Fields*, Appl. Math. Sci. 42, Springer, New York, 1983.

[20] A. Guillamon and G. Huguet, *A computational and geometric approach to phase resetting curves and surfaces*, SIAM J. Appl. Dyn. Syst., 8 (2009), pp. 1005–1042.

[21] F. C. Hoppensteadt and E. M. Izhikevich, *Weakly Connected Neural Networks*, Springer, New York, 1997.

Copyright © by SIAM. Unauthorized reproduction of this article is prohibited.

Downloaded 11/08/19 to 160.36.59.48. Redistribution subject to SIAM license or copyright; see http://www.siam.org/journals/ojsa.php

[22] E. R. Hunt, *Stabilizing high-period orbits in a chaotic system: The diode resonator*, Phys. Rev. Lett., 67 (1991), pp. 1953–1955.
[23] E. A. Jackson and I. Grosu, *An open-plus-closed-loop (OPCL) control of complex dynamic systems*, Phys. D, 85 (1995), pp. 1–9.
[24] D. Jordan and P. Smith, *Nonlinear Ordinary Differential Equations: An Introduction for Scientists and Engineers*, Oxford Texts Appl. Eng. Math. 10, Oxford University Press, Oxford, 2007.
[25] T. Kato, *Perturbation Theory for Linear Operators*, Springer, New York, 1995.
[26] D. Kirk, *Optimal Control Theory*, Dover, New York, 1998.
[27] R. Lima and M. Pettini, *Suppression of chaos by resonant parametric perturbations*, Phys. Rev. A, 41 (1990), 726.
[28] E. N. Lorenz, *Deterministic nonperiodic flow*, J. Atmos. Sci., 20 (1963), pp. 130–141.
[29] J. Moehlis, E. Shea-Brown, and H. Rabitz, *Optimal inputs for phase models of spiking neurons*, J. Comput. Nonlinear Dynam., 1 (2006), pp. 358–367.
[30] E. Ott, C. Grebogi, and J. A. Yorke, *Controlling chaos*, Phys. Rev. Lett., 64 (1990), 1196.
[31] O. Popovych, C. Hauptmann, and P. Tass, *Effective desynchronization by nonlinear delayed feedback*, Phys. Rev. Lett., 94 (2005), 164102.
[32] K. Pyragas, *Continuous control of chaos by self-controlling feedback*, Phys. Lett. A, 170 (1992), pp. 421–428.
[33] K. Pyragas and V. Novičenko, *Time-delayed feedback control design beyond the odd-number limitation*, Phys. Rev. E, 88 (2013), 012903.
[34] V. Pyragas and K. Pyragas, *Delayed feedback control of the Lorenz system: An analytical treatment at a subcritical Hopf bifurcation*, Phys. Rev. E, 73 (2006), 036215.
[35] M. Ramesh and S. Narayanan, *Chaos control by nonfeedback methods in the presence of noise*, Chaos Solitons Fractals, 10 (1999), pp. 1473–1489.
[36] W. Rappel, F. Fenton, and A. Karma, *Spatiotemporal control of wave instabilities in cardiac tissue*, Phys. Rev. Lett., 83 (1999), 456.
[37] J. A. Sanders, F. Verhulst, and J. Murdock, *Averaging Methods in Nonlinear Dynamical Systems*, 2nd ed., Springer, New York, 2007.
[38] S. J. Schiff, K. Jerger, D. H. Duong, T. Chang, M. L. Spano, and W. L. Ditto, *Controlling chaos in the brain*, Nature, 370 (1994), pp. 615–620.
[39] E. Scholl and H. G. Schuster, *Handbook of Chaos Control*, 2nd ed., Wiley-VCH, Weinheim, Germany, 2008.
[40] J. M. Seoane, S. Zambrano, S. Euzzor, R. Meucci, F. T. Arecchi, and M. A. F. Sanjuán, *Avoiding escapes in open dynamical systems using phase control*, Phys. Rev. E, 78 (2008), 016205.
[41] S. Shirasaka, W. Kurebayashi, and H. Nakao, *Phase-amplitude reduction of transient dynamics far from attractors for limit-cycling systems*, Chaos, 27 (2017), 023119.
[42] K. C. A. Wedgwood, K. K. Lin, R. Thul, and S. Coombes, *Phase-amplitude descriptions of neural oscillator models*, J. Math. Neurosci., 3 (2013), 2.
[43] S. Wiggins, *Introduction to Applied Nonlinear Dynamical Systems and Chaos*, Vol. 2, Springer, New York, 2003.
[44] C. Wilson, B. Beverlin II, and T. Netoff, *Chaotic desynchronization as the therapeutic mechanism of deep brain stimulation*, Front. Syst. Neurosci., 5 (2011), 50.
[45] D. Wilson, *Isostable reduction of oscillators with piecewise smooth dynamics and complex Floquet multipliers*, Phys. Rev. E, 99 (2019), 022210.
[46] D. Wilson and B. Ermentrout, *Greater accuracy and broadened applicability of phase reduction using isostable coordinates*, J. Math. Biol., 76 (2018), pp. 37–66.
[47] D. Wilson and B. Ermentrout, *An operational definition of phase characterizes the transient response of perturbed limit cycle oscillators*, SIAM J. Appl. Dyn. Syst., 17 (2018), pp. 2516–2543.
[48] D. Wilson and J. Moehlis, *Optimal chaotic desynchronization for neural populations*, SIAM J. Appl. Dyn. Syst., 13 (2014), pp. 276–305.
[49] D. Wilson and J. Moehlis, *Isostable reduction of periodic orbits*, Phys. Rev. E, 94 (2016), 052213.
[50] A. Winfree, *The Geometry of Biological Time*, 2nd ed., Springer, New York, 2001.

Downloaded 11/08/19 to 160.36.59.48. Redistribution subject to SIAM license or copyright; see http://www.siam.org/journals/ojsa.php

Copyright © by SIAM. Unauthorized reproduction of this article is prohibited.